




Polymeric smart coatings containing modified capped halloysite nanotubes for corrosion protection of carbon steel

Sehrish Habib^{1,2}, Adnan Khan³, Salman M. Ismail⁴, R. A. Shakoor^{1,2,*} , Ramazan Kahraman^{5,*}, and Elsadig Mahdi Ahmed²

¹Center for Advanced Materials (CAM), Qatar University, 2713 Doha, Qatar

²Department of Mechanical and Industrial Engineering, Qatar University, 2713 Doha, Qatar

³Department of Materials Science and Engineering, Texas A&M University, College Station, TX 77843, USA

⁴Community College of Qatar, Doha, Qatar

⁵Department of Chemical Engineering, Qatar University, 2713 Doha, Qatar

Received: 18 January 2023

Accepted: 23 March 2023

© The Author(s) 2023

ABSTRACT

A newly designed smart self-healing epoxy coating system comprised of modified halloysite nanotubes (HNTs) having capping is proposed for corrosion protection of steel. In the first step, HNTs were loaded with 8-hydroxyquinoline (8HQ), used as a corrosion inhibitor. Then the HNTs were sealed/capped using cobalt (II), aiming for an efficient and controlled release of the loaded inhibitor. The smart coatings were developed by reinforcing loaded HNTs into the epoxy matrix. The structural, thermal, mechanical, and electrochemical properties of capped modified HNTs and smart coatings were studied using various techniques. UV–Vis analysis depicted that the capping of the metal-inhibitor complex was decomposed at acidic pH resulting in a controlled release of the loaded inhibitor into HNTs. Electrochemical impedance spectroscopic (EIS) analysis of blank and smart coatings demonstrated that the low-frequency impedance modulus of smart coatings is $10^9 \Omega \cdot \text{cm}^2$ for 20 days compared to blank coatings ($10^5 \Omega \cdot \text{cm}^2$), reflecting their excellent corrosion inhibition performance. The superior corrosion protection properties of these smart coatings can be ascribed to the controlled and efficient release of the loaded inhibitor from the capped HNTs. Finally, X-ray photoelectron spectroscopy (XPS) analysis of the steel substrate after the corrosion analysis revealed the adsorption of 8HQ on the steel surface, confirming the formation of iron complex due to the release of loaded inhibitor. This work demonstrated the adeptness of 8HQ in mitigating the corrosion due to the controlled and effective release of the inhibitor from capped HNTs because of dissociation of the metal-inhibitor complex (Co-8HQ).

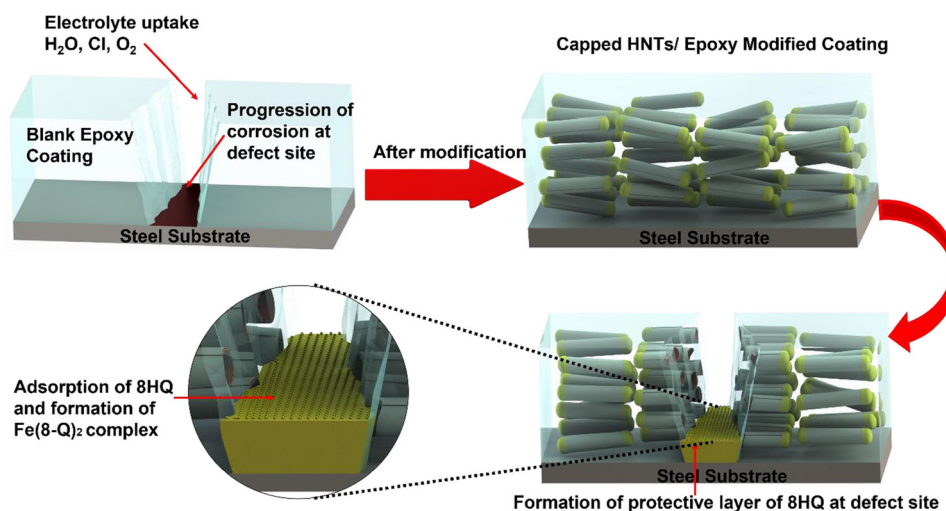
Handling Editor: Maude Jimenez.

Address correspondence to E-mail: shakoor@qu.edu.qa; ramazank@qu.edu.qa

<https://doi.org/10.1007/s10853-023-08437-z>

Published online: 10 April 2023

GRAPHICAL ABSTRACT



Introduction

Corrosion is one of the most common causes of metal failure in industrial equipment. Damage from corrosion can shut down industrial processes, subsequently causing economic losses [1]. For this reason, corrosion control has become a significant focus in various industries [2, 3]. Corrosion prevention is often carried out by selecting appropriate corrosion-resistant material, corrosion inhibitors, cathodic protection, and protective coatings. The polymeric coating is one of the most efficient methods used on metals to restrict the corrosion process [4]. However, despite having significant corrosion prevention capabilities, the coating layer can easily be damaged for various reasons, including changes in environmental conditions throughout its service life. This damage to the protective coating can expose the metal to a corrosive environment and enable the spread of corrosion. Such damage can occur as cracks on a micro-scale which is challenging to detect and facilitates corrosion propagation in metals [4, 5].

Corrosion inhibitors can be added to the coating to prevent corrosion propagation in the cracked region [6]. Such coating possesses self-healing properties

and refers to smart coating [7]. Inhibitors can be added directly to the coating or loaded into nanocontainers before mixed into the resin matrix [8–12]. Directly adding inhibitors has proven to compromise the strength of the coating as they dissolve with water over time. Furthermore, the inhibitors can also react with the polymeric matrix resulting in cavities in the coating, subsequently reducing its strength [13]. Whereas in the case of nanocontainers, the inhibitors are preserved in nanocontainers and released upon coating damage that exposes the nanocontainers to corrosive ions [14]. Hence, nanocontainers are more effective in inhibitor preservation [15]. Tubular nanocontainers are more hydrodynamic than spherical shaped capsules because of their proper orientation, proper aspect ratio and comparable density with polymeric matrix; therefore, they provide better process ability and disperse more uniformly when added as filler in nanocomposites [16].

Halloysite nanotube (HNT) is a highly preferred candidate for smart coating. HNTs are inorganic materials chemically the same as kaolinite, where a layer of water separates the layers. HNTs are naturally found in the USA, Australia, New Zealand, Brazil, Mexico, and China, having a chemical formula of $\text{Al}_2(\text{OH})_4\text{Si}_2\text{O}_5 \cdot n\text{H}_2\text{O}$ and are found in various

morphological forms including spheroidal, tubular, and platy. The most dominant morphology found in HNTs is tubular. The tubular HNTs have a hollow structure with an inner diameter ranging between 10 to 100 nm and an outer diameter ranging between 30 and 100 nm—the length of HNTs range between 0.1 μm and 3 μm . HNTs can store inhibitors, whereas end stoppers are used to control the release of inhibitors [17–19]. Since HNTs are biocompatible and non-toxic, they are also used in biotechnological applications such as controlled drug release and tissue engineering [20, 21].

The kaolin sheets in HNTs are rolled as layers with SiO_2 layers on the external surface and Al_2O_3 in the inner layer. Therefore, the outer layer has a weak negative charge, and the inner layer has a strong positive charge. Reducing the pH under 8.5 will switch these charges such that the inner lumen is positively charged, and the outer surface is negatively charged. This enables the loading of negatively charged species inside the HNTs [22]. The corrosion inhibitor can be loaded into HNT either by soaking them in an inhibitor solution or by agitating the suspension of capsules and fillers. The loading mechanism varies based on the nature of the compound. These are either direct loading or salinization loading mechanisms [23, 24].

It takes initial 5 to 10 h to release a compound from a clay nanotube [25]. The release time is increased based on the application. The release of the encapsulated compound can be controlled under specific external stimuli such as pH or temperature of its environment and diameter of internal tube of HNT [26]. Sometimes the compound must be released by targeting a particular region, making the release rate control ever more significant. End stoppers are used to control the release rate [27]. Maria R. Dzamukovause et al. [28] used dextrin as an end stopper that enabled a targeted release of compounds to cancer cells. Similarly, in the case of cracks in coating, an end stopper can allow the targeted release of corrosion inhibitor to the crack region [29]. End stoppers can be made either by forming urea formaldehyde on the HNT surface, layer-by-layer encapsulation or forming a metal-inhibitor complex. Xuteng Xing et al. [30] loaded HNTs with Na_2MoO_4 as a corrosion inhibitor and controlled the release rate of the inhibitor by modifying HNTs with Ca^{2+} due to the formation of CaMoO_4 . The metal-inhibitor complex was decomposed at acidic pH. The EIS analysis demonstrated

good corrosion inhibition performance of epoxy coatings modified with 10 wt.% of Ca^{2+} modified HNTs. It was also concluded that the concentration of metal ions is inversely proportional to the release rate of benzotriazole. Mei Wang et al. [31] synthesized Cu-8HQ@HNT/epoxy coatings to study the corrosion inhibition performance of steel substrate due to the controlled release of 8HQ. The EIS results of the epoxy modified with Cu-8HQ@HNT showed the corrosion resistance of $10^5 \Omega \cdot \text{cm}^2$ which was higher than that of blank epoxy coating.

In our work, we aimed to load pristine HNTs with 8HQ and their modification with Co (II) cap for controlled release of inhibitor by pH variations. 8HQ was utilized explicitly due to the presence of nitrogen. The nitrogen of the quinoline ring has an affinity for bonding with empty d-orbitals of iron of steel substrate and due to the high electron density. 8HQ is expected to have good interaction with metal surface thus forming passive protective layer on the metal surface. Also due to the presence of highly polar functional group at 8th position they form highly stable chelating compound with metal surface thus protecting metal against corrosion even at low concentration [32, 33]. Quinoline and its derivatives are highly soluble in aqueous phase which is why they are also considered as environmental sustainable corrosion inhibitor [34, 35]. The choice of Co (II) in this system is because Co (II) resulted in the formation of more stable complexes than its comparative series transition metals, such as Cu (II) and Ni (II) [36]. The morphological, structural, and self-release behavior was also analyzed and revealed. The formation and decomposition mechanism of capping of HNTs was also demonstrated and confirmed. EIS technique was employed to study the corrosion inhibition performance of blank epoxy coatings and smart coatings. The epoxy coatings modified with capped HNTs showed decent barrier properties and improved performance against corrosion of steel in 35 g/L NaCl solution.

Experimental

Reagents used

Halloysite nanotubes (HNTs) used as nanocarrier and 8-hydroxyquinoline (8HQ) used as corrosion inhibitor were procured from Sigma-Aldrich, Germany. Cobalt sulfate heptahydrate ($\text{CoSO}_4 \cdot 7\text{H}_2\text{O}$) was utilized to make capping of HNTs, and other

reagents used, e.g., sodium chloride, ethanol, hydrochloric acid, were also purchased from Sigma-Aldrich. Epoxy resin (EPON 815C) and its curing agent (EPIKURE) were acquired by Hexion Chemical. Carbon steel ($35 \times 35 \text{ mm}^2$) utilized as substrates (with composition of $C = 0.21\%$, $P = 0.30\%$, $S = 0.04\%$, $Cu = 0.20\%$ and $Fe = 99.18\%$ and thickness of 1 mm) were procured from a local supplier. Silicon carbide abrasive paper was obtained from Hebei Yineng pipeline Group Co., Ltd, China.

Modification of HNTs with corrosion inhibitor (8HQ)-Uncapped HNTs

To load 8HQ in HNTs, a saturated solution of 8HQ was prepared by mixing 8HQ in ethanol. Pristine HNTs were added into a saturated solution of 8HQ. This solution was then placed overnight, stirring at $25 \text{ }^\circ\text{C}$ @ 500 rpm. A beaker comprising corrosion inhibitor and HNTs suspension was later transferred to the vacuum chamber and connected to the vacuum pump. Vacuum cycling was performed so that suspension was placed in a chamber for 1 h in full vacuum conditions, and later vacuum was removed to atmospheric pressure. This process was repeated 3 to 4 times to enhance loading capacity. This process ensured that air was drawn entirely from HNTs lumen and replaced by corrosion inhibitor. The suspension was then transferred for centrifugation at 5000 rpm for 15 min to separate modified HNTs from the solution. The product was later dried at $60 \text{ }^\circ\text{C}$ for 20 h. The resultant product was ground to a fine powder in mortar and pestle. Two types of samples were collected from the product. One was labeled as uncapped HNTs, and the other underwent a capping process hereafter and was labeled as capped HNTs.

Capping formation

To control the release of the inhibitor from HNTs, capping was done. For this purpose, modified HNTs were exposed to the 0.5 M bulk aqueous solution of $\text{CoSO}_4 \cdot 7\text{H}_2\text{O}$ comprising Co (II) ions for 1 min with continuous stirring. This process is based on the reaction between corrosion inhibitor and Co from aqueous solution, which is then diffused into HNTs opening to form Co-8HQ complex on the HNT tube later. The resultant solution was then centrifuged at 5000 rpm for 10 min, followed by drying to get dried powder. The formation

of capping and their chemical bonding are represented in Fig. 1.

Preparation of steel substrate

Carbon steel coupons obtained from a local source were polished by employing a grinding and polishing machine (Metkon ForcoPol IV) utilizing silicon carbide abrasive paper (120c). The polished steel substrate was then cleaned with ethanol or acetone to remove any residue or prevent any iron oxide layer formation. The cleaned samples then proceeded to the epoxy coating procedure.

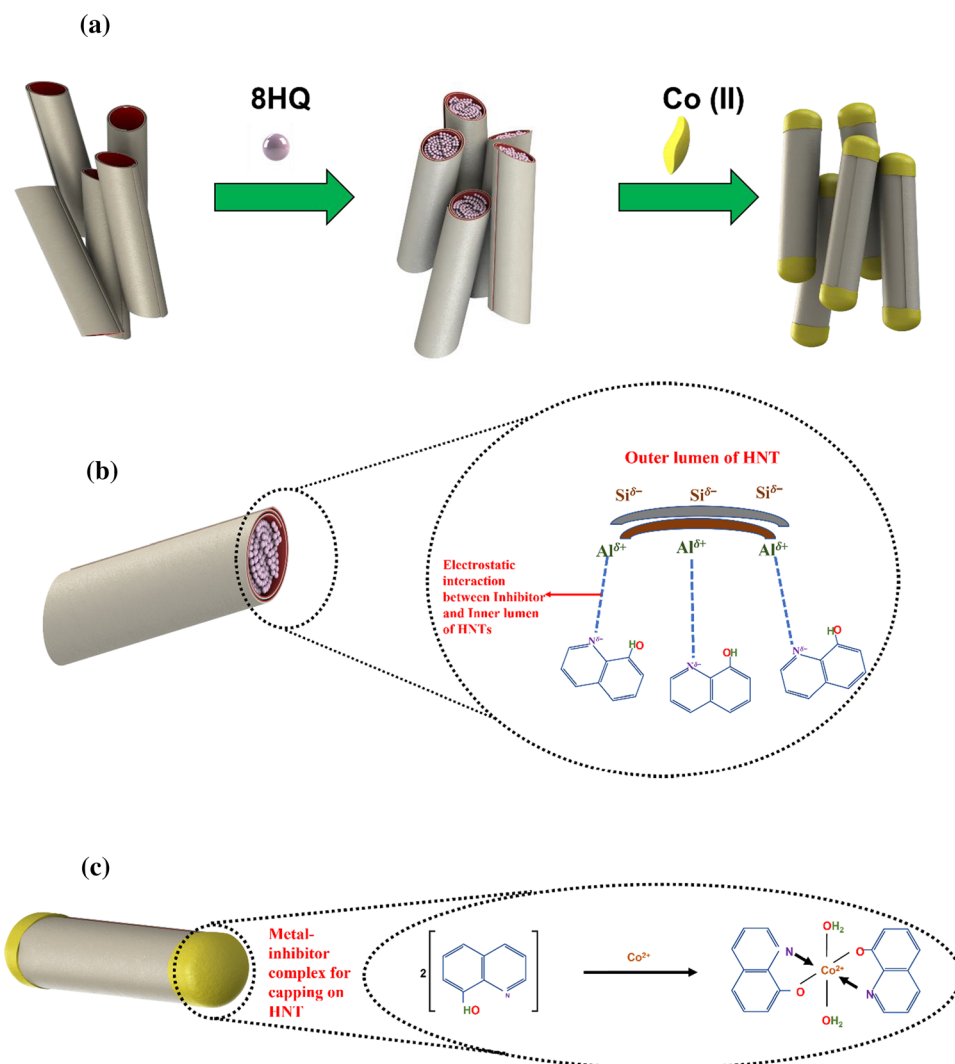
Synthesis of epoxy-based nanocomposite smart coating

Two different types of reinforced coatings were developed. (i) Blank epoxy coating (without any additive or modifications) is referred to as reference coating synthesized for comparison purposes. (ii) Epoxy coating reinforced with capped HNTs is referred to as capped HNTs/Epoxy coating. To prepare coatings, first reference coatings were formulated. For this purpose, 4 gm of epoxy was mixed with 1 gm of its curing agent. The doctor blade technique deposited the coating mixture on the steel substrate. To formulate modified coatings, 1 wt.% (with respect to epoxy weight) of modified HNTs particles were added to 4 gm of epoxy in a beaker and left on stirring for 5 min at 500 rpm. Later, 1 gm of curing agent was added to the mixture and again stirred for 5 min for better dispersal of modified particles and to remove air bubbles. The synthesized modified coating mixture was then deposited on a steel substrate similarly to reference coatings. The prepared coatings (reference and modified) were then left for curing at room temperature for ten days for complete curing before the initiation of corrosion inhibition performance testing via EIS. The final thickness of coatings (assessed by PosiTector 6000) from DeFelsko) was $75 \pm 5 \text{ }\mu\text{m}$. A manual scratch was made on the developed coating using a scalpel.

Characterization of synthesized particles and epoxy reinforced smart nanocomposite coatings

Transmission electron microscope (TEM, FEI, TALOS F200X, USA) and field emission scanning electron

Figure 1 Schematics showing **a** Modification of HNTs with corrosion inhibitor and capping **b** Electrostatic interactions between inner lumen of HNTs and inhibitor **c** Formation of the metal-inhibitor complex to form caps.



microscope (FE-SEM-Nova Nano-450, FEI, New York, NY, USA) combined with EDS tool were utilized for morphological analysis of Pristine HNTs, uncapped and capped HNTs. An organic elemental analyzer (Flash 2000 Elemental Analyzer (CHNS/O)) was employed to analyze the carbon, nitrogen, and hydrogen weight percentage of the uncapped and capped HNTs. FTIR Frontier (PerkinElmer, Waltham, MA, USA) spectrometer in the range of 4000–500 cm^{-1} was employed to analyze the chemical interaction between HNTs, corrosion inhibitors, and caps. To study the mass loss associated with the thermal stability of pristine HNTs, uncapped and capped HNTs, thermogravimetric analysis and differential thermal gravimetric analysis (DTA) (pyris 4000 PerkinElmer-USA) in the range of 30–1000 $^{\circ}\text{C}$ with the heating rate of 10 $^{\circ}\text{C}/\text{min}$ under nitrogen environment were employed. Specific surface area

and cumulative pore volume of pristine HNT before and after loading and capping were studied using Brunauer–Emmett–Teller (BET) (Surface Area Analyzer, Micromeritics ASAP 2420, USA). X-ray diffraction analysis (PANanalytical, Empyrean, Royston, United Kingdom) X'pert Pro Cu (K α) with a scanning rate of 2 $^{\circ}/\text{min}$ and scanning angle ranging between 10 $^{\circ} \leq 2\theta \leq 90^{\circ}$ was employed to study the structural and phase purity of pristine HNTs, uncapped and capped HNTs. To study uncapped and capped HNTs in 35 g/L NaCl solution, UV–Vis spectroscopic analysis (Biochrome Libra S60 double beam spectrophotometer, United Kingdom) was employed. To analyze the release percentage of uncapped and capped HNTs, a small amount of both were dissolved in a 35 g/L NaCl solution. A small amount of capped HNTs was added to 35 g/L NaCl solution at different pH (2, 5, 7, 9, 11). The pH of the

solution was adjusted by adding HCl or NaOH dropwise until the desired pH was obtained. Tensile testing of the synthesized coatings was achieved by utilizing a Universal testing machine (Lloyd-Ametek LR50K Plus, USA). An engineering strain rate of 10^{-4} /s under uniaxial tensile loadings was applied to study the tensile behavior of the synthesized coatings, and explanation has been added into supplementary data.

Electrochemical impedance spectroscopic analysis was conducted to study synthesized coatings' corrosion inhibition performance in 35 g/L NaCl solution at 25 °C. The considerable frequency range was 0.01 Hz to 100 kHz by employing Gamry 3000 apparatus (30 K BOOSTER potentiostat/galvanostat/ZRA, USA). The Gamry instrument utilized a three-electrode system. Coated steel substrate was used as the working electrode (exposed area of 0.765 cm²), Ag/AgCl as the reference electrode, and graphite as the counter electrode. A scratch of about 160 μm was made manually using a scalpel on a coated steel substrate. The steel substrate was then immersed in 35 g/L NaCl solution, and impedance testing was done for 1, 5, 10, 15, and 20 days. The testing was repeated thrice on each sample to generate consistent results. XPS (AXIX Ultra DLD, Kratos, UK) using a monochromatic X-ray source—Al K α source was employed to study the surface of modified coating after 20 days of immersion. The spectra were recorded to evaluate elemental composition in the 250 to 750 eV binding energy range.

Results and discussion

Morphological and structural analysis

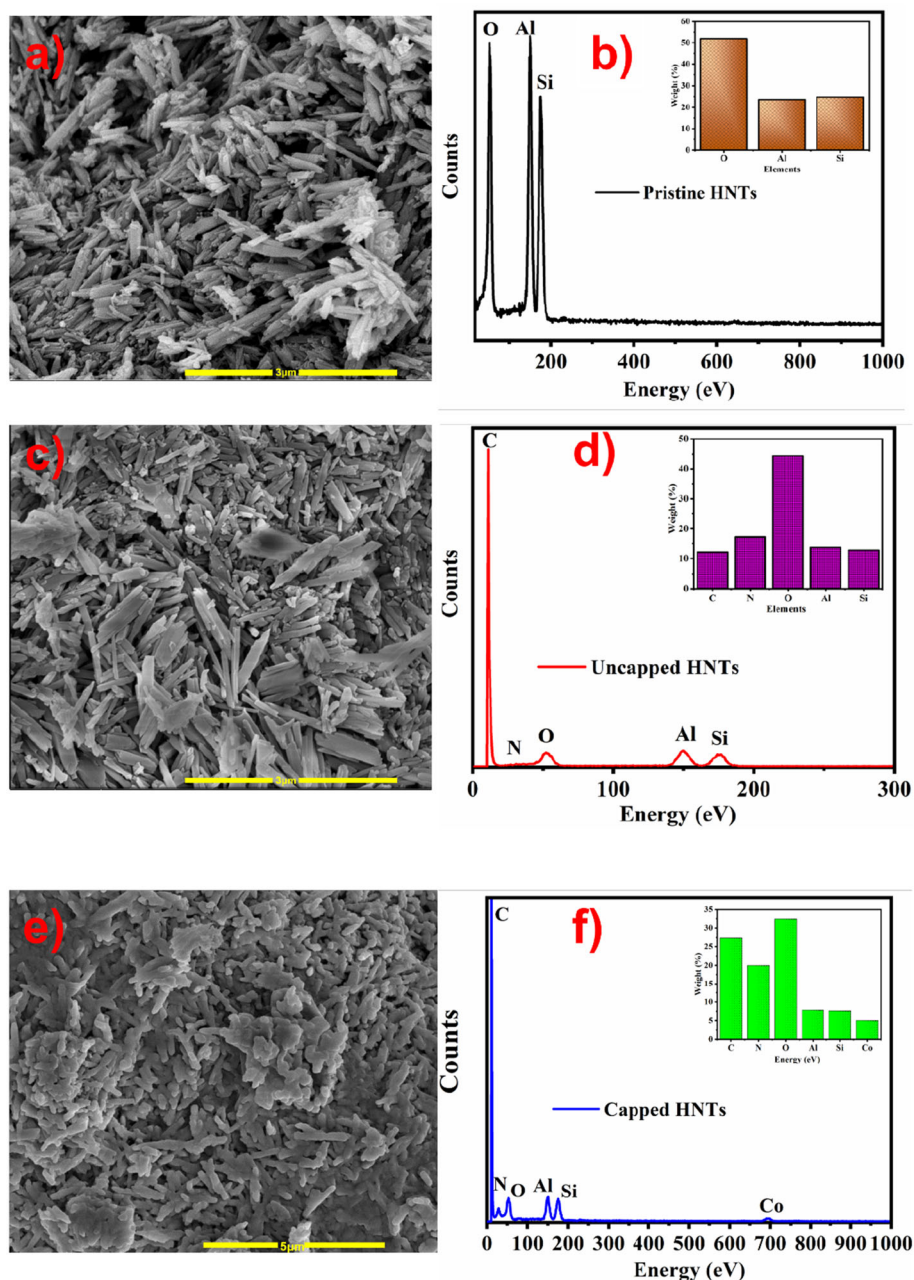
SEM, TEM and EDX analysis

Figure 2 represents the FE-SEM and EDX analysis of pristine HNTs (Fig. 2a, b), uncapped HNTs (Fig. 2c, d), and capped HNTs (Fig. 2e, f). FE-SEM of pristine HNTs (Fig. 2a) represented the rolled tubular structure with a hollow inner lumen which is more evident in TEM images (Fig. 3). It is also apparent from SEM analysis that HNTs comprise crushed pieces of tubes, making them attractive as nanocarriers [37]. EDX analysis of pristine HNTs (Fig. 2b) confirmed the presence of alumina, oxygen, and silica, which are the main elements of HNTs

(Al₂Si₂O₅(OH)₄·2H₂O) [38]. After modification of HNTs with 8HQ (corrosion inhibitor) and caps, it is evident that the morphology of HNTs remained unchanged, and the surface is still smooth, as shown in Fig. 2c and e. However, the emergence of a few clusters is evident in Fig. 2c, e, which may be due to the loading of inhibitors and the formation of a cap on the outer wall of HNTs [39]. It is also apparent from EDX analysis of uncapped and capped HNTs (Fig. 2d, f) that 8HQ is successfully loaded in HNTs. The main elements of 8HQ can be seen in the EDX analysis. In the case of capped HNTs, small amount of Co is also seen, demonstrating that the caps are present and formed. Pristine HNTs have a positively charged internal layer of aluminum hydroxide (Al(OH)₃) and external surface layer of negatively charged silica (SiO₂) [4] which makes them a particular carrier for both positively and negatively charged species. The internal positively charged layer attracts a negatively charged inhibitor (8HQ) as the net charge on 8HQ is negative [40].

TEM analysis of pristine, uncapped, and capped HNTs is represented in Fig. 3. Figure 3a, b represents the pristine HNTs images with the hollow inner lumen. Figure 3c demonstrates the loading of 8HQ into the inner layer of HNTs. Some dark areas are also revealing that 8HQ is successfully loaded into HNTs. The cap formation is more evident in TEM analysis (Fig. 3d). TEM images of Fig. 3d show the formation of a cap on HNTs, which is developed due to the formation of metal (Co)-inhibitor complex on HNTs. Organic elemental analysis was done to study the carbon, nitrogen, and hydrogen content in uncapped and capped HNTs. The results demonstrated that uncapped HNTs consisted of nitrogen (17.98%), carbon (12.34%), and hydrogen (2.17%), while in capped HNTs, the weight percentage of nitrogen, carbon, and hydrogen were 19.25, 27.18, and 2.89%, respectively. It is evident from these results that corrosion inhibitor is successfully loaded into HNTs. EDX results (Fig. 2) also endorsed these results by revealing the presence of the main elements of corrosion inhibitor and cap. Elemental mapping (Fig S1) was also done to confirm the formation of capping on HNTs. The elemental mapping results showed that the Co (II) is not only present on the ends of HNTs but more prominently covered the surface of HNTs as represented in TEM images as well.

Figure 2 SEM and EDX analysis of pristine HNTs (a, b), uncapped HNTs (HNTs/8HQ) (c, d), and capped HNTs (e, f).

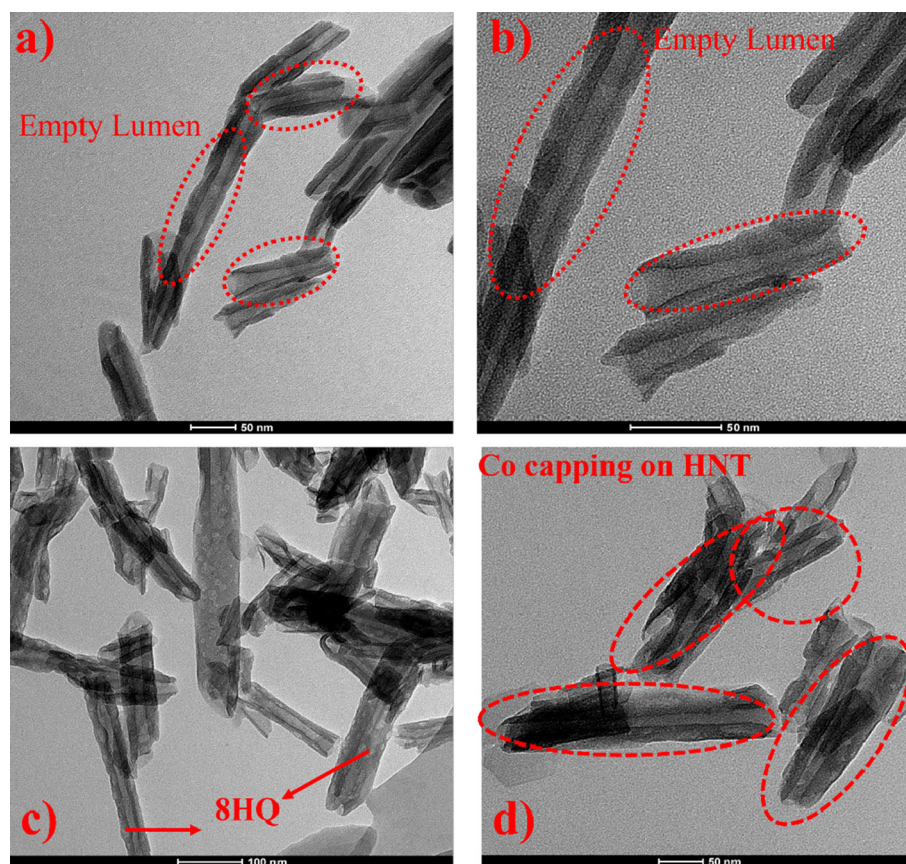


FTIR analysis

Figure 4a demonstrates the FTIR analysis of pristine HNTs, uncapped and capped HNTs. In the case of pristine HNTs, the prominent absorption bands are observed at 3697, 3614, 1111, 1020, 908, and 538 cm^{-1} . The absorption band observed at 3697, and 3614 cm^{-1} is attributed to the Al–OH bond stretching [39, 41]. The peaks at 1111 and 1020 cm^{-1} are attributed to the perpendicular and in-plane Si–O–Si bond stretching. The characteristic peak at 908 and

538 cm^{-1} is ascribed to the bending vibrations for Al_2OH bond deformation and bending vibrations of Si_2O bond [41, 42]. In the case of uncapped HNTs and the characteristics peak of HNTs, some of the distinctive peaks of 8HQ are also seen. The distinctive peaks of 8HQ are observed at 1567, 1459, 1276, 787, and 743 cm^{-1} . The peak at 1567 cm^{-1} demonstrates the C = N ring stretching vibrations. The absorption bands at 1459 cm^{-1} and 1276 cm^{-1} represent O–H plane bending and C–O stretching vibrations. The O–H and C–H out of plane bending appeared at 787 and

Figure 3 TEM analysis of **a**, **b** pristine HNTs, **c** uncapped HNTs, and **d** capped HNTs.



743 cm^{-1} [43]. The absorption band in capped HNTs spectra are similar to the uncapped ones; however, there is the appearance of a peak at 567 cm^{-1} , which is attributed to the metal(II)-nitrogen bond (Co-Inhibitor complex) [20]. The appearance of this peak is an indication of the formation of the metal-inhibitor complex on HNTs.

XRD analysis

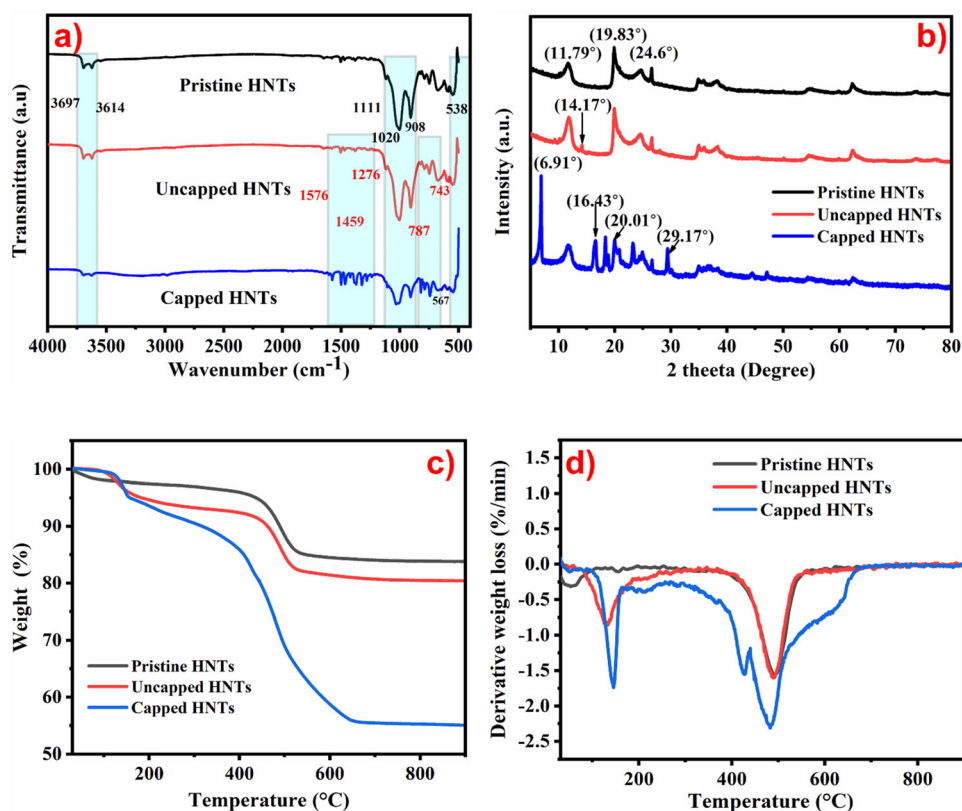
XRD analysis of pristine HNTs, uncapped and capped HNTs is demonstrated in Fig. 4b. Pristine HNTs represented the characteristic diffraction peaks at 11.79° , 19.83° , and 24.6° with corresponding crystal planes of (001), (100), and (002), respectively [44]. After loading pristine HNTs with 8HQ, the XRD pattern revealed no new peak except one peak at 14.17° , which corresponds to that of 8HQ [45]. However, the peaks represented the shift of ± 0.10 to the right side, demonstrating that some disturbance in the structure of HNTs is seen due to the intercalation of 8HQ into HNTs. Similar behavior has been seen in the case of capped HNTs. However, some

addition peaks represent the formation of metal-inhibitor complexes such as at 6.91° , 16.43° , 20.01° , and 29.17° , demonstrating the formation of cobalt (bis-8-hydroxyquinoline) (CoQ_2) complex on HNTs [46].

TGA and DTA analysis

TGA and DTA analysis of pristine HNTs, and uncapped and capped HNTs are represented in Fig. 4 (c, d). TGA analysis of pristine HNTs (Fig. 4c) reveals an initial mass loss of 4% due to the presence of water content in the interlayer of the product [47]. This mass loss is seen from 100 to 97°C . The small endothermic peak in this region in the DTA analysis of pristine HNTs (Fig. 4 d) demonstrates the same mass loss due to interlayer water content. After removing water, the product remained relatively stable up to 400°C . After 400°C , the prominent degradation peak is seen in the TGA analysis of HNTs, which demonstrates the dihydroxylation of HNTs. In this step, the product decomposed, and the OH group was released from Al^{3+} ions to form meta halloysite. This degradation of HNTs is an

Figure 4 **a** FTIR analysis of pristine HNTs, uncapped HNTs, and capped HNTs, **b** XRD analysis of pristine HNTs, uncapped and capped HNTs, **c** Thermogravimetric analysis and **d** differential thermal gravimetric analysis of pristine HNTs, uncapped and capped HNTs.



endothermic reaction, and a strong endothermic peak can be seen in the DTA (Fig. 4d) analysis of pristine HNTs [48]. Almost 12–14% of mass loss has been observed in this region. In the case of TGA analysis of uncapped HNTs (Fig. 4c), the slight mass loss seen from 110 to 222 °C is due to the degradation of 8HQ loaded into HNTs. This can be seen in the DTA curve (Fig. 4d). A strong endothermic peak is observed, which reveals the degradation of 8HQ. In the third stage of the TGA analysis, the degradation followed after 400 °C demonstrates the decomposition of HNTs, which can also be seen in the DTA analysis. Almost 19% of mass loss is seen at this stage. The TGA analysis of capped HNTs demonstrates similar behavior to uncapped HNTs. However, the degradation of 8HQ is seen at 156 °C higher than that of 110 °C seen in uncapped HNTs. This may be due to the formation of Co-8HQ complex. The mass loss seen in the region of 200 to 650 °C is associated with Co (II) complexes. A total of 45% of mass loss is seen in this region. The metal complexes demonstrated a fast and huge mass loss because the disintegration of chelates is catalytically stimulated by metal (II) ions [49, 50].

BET analysis

The N₂ adsorption and desorption isotherms representing the BET analysis of pristine HNTs, and uncapped and capped HNTs are illustrated in Figure S2. BET analysis of pristine HNTs, uncapped and capped HNTs is also demonstrated in Table 1. The BET analysis in Figure S2 represents a loop type of curve, which indicates mesoporous and microporous structures [39]. The specific surface area (SSA) and pore volume (PV) of all the samples showed a gradual decrease. The SSA and PV of pristine HNTs come out to be 99.46 m²/g and 0.56 cc/g. The SSA of pristine HNTs has decreased to 76.51 and 70.44 m²/g, and PV has been reduced to 0.34 and 0.33 cc/g for uncapped and capped HNTs, respectively. The significant decrease in SSA and PV endorses the loading of 8HQ in HNTs [39, 51]. The further reduction in SSA and PV of capped HNTs indicates adsorption of metal and the formation of a metal-inhibitor bond on HNTs.

Table 1 Specific surface area and pore volume of pristine HNTs, uncapped and capped HNTs

Sample name	Specific surface area (m ² /g)	Pore volume (cc/g)
Pristine HNTs	99.46	0.54
Uncapped HNTs	76.51	0.34
Capped HNTs	70.44	0.33

UV-Vis spectroscopic analysis for release studies

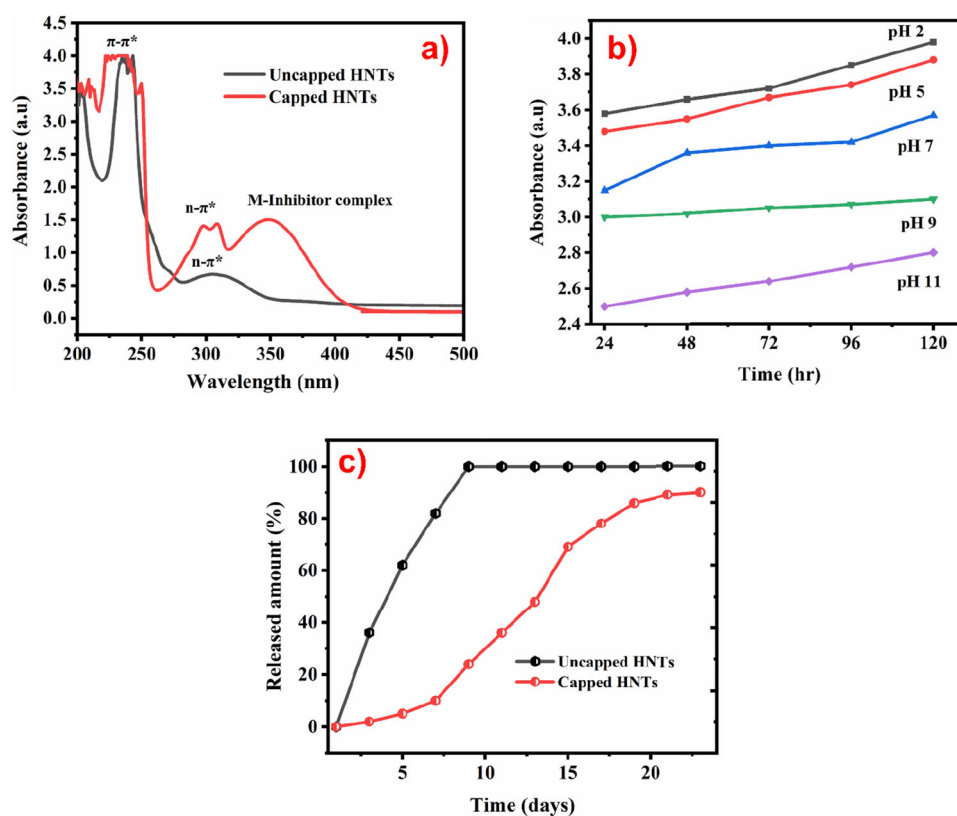
UV-Vis spectroscopic analysis was done for uncapped and capped HNTs at pH 2. As represented in Fig. 5a, we can see two primary UV spectra at pH 2. The spectra for uncapped HNTs represent two main absorption peaks at 234 and 308 nm, demonstrating $\pi-\pi^*$ and $n-\pi^*$ transition in the quinoline ring [20]. The absorption spectra of capped HNTs represent three main absorption peaks at 237, 310, and 370 nm. The peaks at 237 and 308 nm are due to the $\pi-\pi^*$ and $n-\pi^*$ transitions in 8HQ, which shifted slightly to a higher wavelength (bathochrome shift) [20]. The peak at 370 nm can be associated with Co (II)-inhibitor charge transfer transitions [52, 53].

The release behavior of inhibitors from HNTs at various pH at 370 nm is represented in Fig. 5b. The figure demonstrates that the release of inhibitors

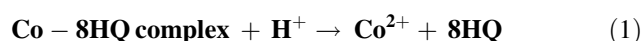
depends on time and pH. As time increases, the intensity of inhibitor released is also increasing. The pH release behavior of the inhibitor shows that the inhibitor represented more release in an acidic medium than in the basic medium. Figure 5c shows the release weight percentages of uncapped and capped HNTs in 35 g/L NaCl solution at various time intervals. The release weight percentages of uncapped HNTs are observed to be finished at nine days, and about 36% of the inhibitor has been released into solution in the first three days, which were loosely attached to the HNTs surface [30]. After nine days, almost all the inhibitor has been released into the solution. But this situation is unwanted. In the case of capped HNTs, the release percentage with time is relatively slow, and release time has been extended.

After three days, only 5% of the physically adsorbed inhibitor had been released, and even after

Figure 5 UV-Vis spectroscopic analysis of **a** uncapped and capped HNTs at pH 2 **b** Release studies of capped HNTs at 370 nm at various pH (2, 5, 7, 9, 11) at different time intervals in 35 g/L NaCl solution **c** Release weight % of 8HQ from uncapped and capped HNTs in 35 g/L NaCl solution at various time intervals.



20 days, not all of the inhibitor was released. The insertion or formation of the cap (Co (II)) on HNTs can prolong the release time of 8HQ. However, in some instances, the inhibitor release significantly inhibits the corrosion process at the defect site. In this case, the metal-inhibitor complex must be decomposed to increase the release of the inhibitor. The acidic medium facilitates cap and inhibitor bond decomposition by releasing the hydrogen ions (H^+) from HCl in the NaCl solution. HCl was added to the solution to maintain acidic pH [54]. This can be explained by Eq. 1.



The release of inhibitors is more pronounced and enhanced in an acidic medium (pH 2 and 5) than in the basic medium (pH 9 and 11). So, in the case of coatings, due to the localized change in the pH at the scratch area, the complex will be decomposed, releasing free metal ions and inhibitors.

Electrochemical analysis of synthesized coatings

The corrosion inhibition efficiency of developed coatings

The electrochemical impedance spectroscopy analysis of developed coatings was performed in 35 g/L NaCl solution over 20 days. Two types of coatings were developed: blank epoxy coatings and epoxy reinforced with capped HNTs (capped HNTs/Epoxy) coatings or smart coatings. Figure 6 represents the equivalent circuit employed for fitting the experimental data acquired from EIS analysis to compute the fundamental electrochemical parameters over 20 days of immersion. The electrochemical parameters comprise R_s (Solution resistance), R_{po} (Pore resistance), R_{ct} (Charge transfer resistance), CPE1 (coating capacitance, CPE2 (double layer capacitance between the steel substrate and NaCl solution), and W (Warburg diffusion coefficient). R_s is the solution resistance attained by the electrolyte (35 g/L NaCl solution). R_p is the resistance offered by the defect (scratch) made in coatings, and R_p along with CPE1 is assessed at a high-frequency time constant. R_{ct} is the resistance acquired by developed coatings, and R_{ct} , along with CPE2, is determined at a low-frequency time constant [39]. The impedance spectra attained at the high-frequency range can be utilized to study the protective behavior of the

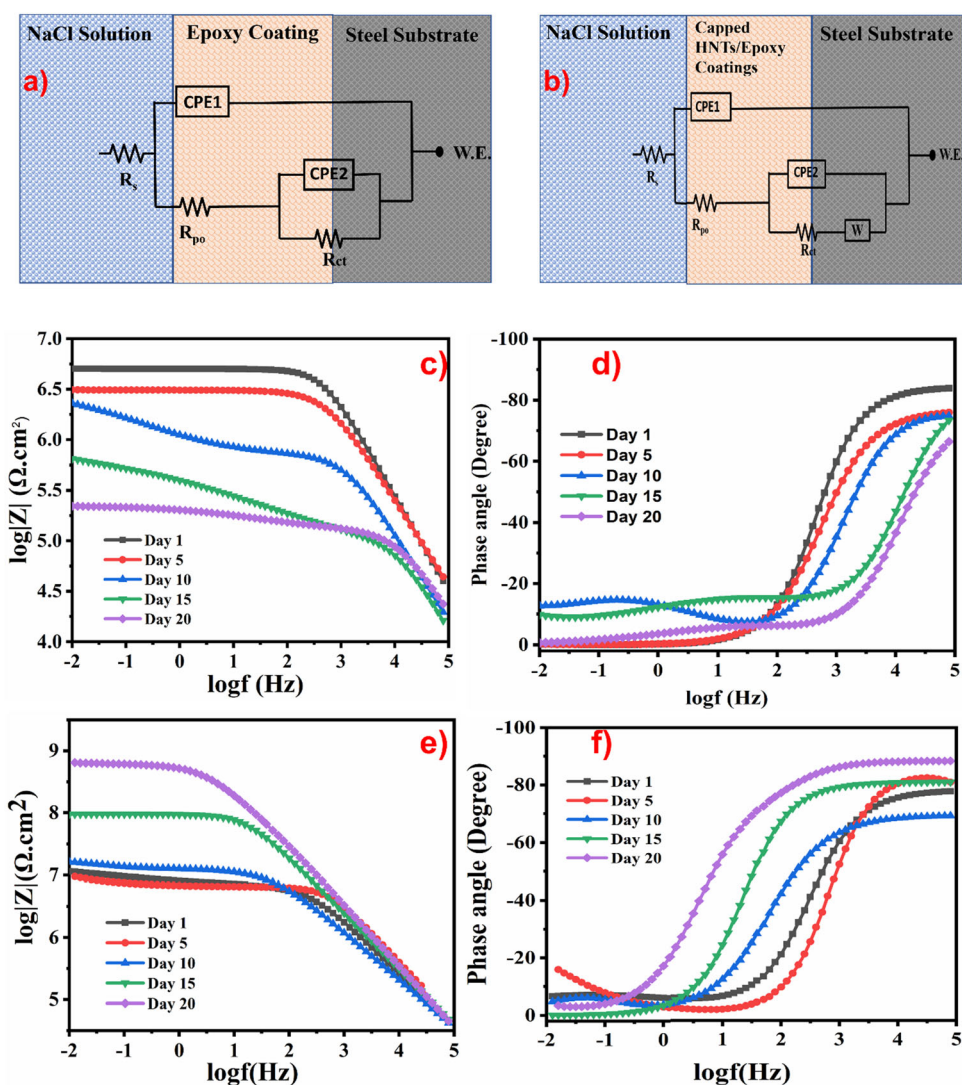
coatings. Two times constant circuit was employed for both types of coatings (blank epoxy and capped HNTs/epoxy), but diffusion constant (W) was introduced in a circuit (Fig. 8b) for capped HNTs/epoxy coatings in EIS data fitting.

Figure 6c, d represents the bode and phase angle plot for blank epoxy and capped HNTs/Epoxy coatings. The detailed values of EIS parameters are provided in (Supplementary Table 2). The scratched blank epoxy coating shows the impedance modulus of $7.38 \text{ M}\Omega\cdot\text{cm}^2$ on 1st day of immersion at a low-frequency range of $|Z_{0.01 \text{ Hz}}|$. As immersion time increases, the corrosion resistance behavior of blank epoxy coating is observed to decrease. On the 10th day of immersion, we can observe that the low-frequency impedance modulus is reduced to $0.171 \text{ M}\Omega\cdot\text{cm}^2$. This gradual decrease in the corrosion protection behavior of blank epoxy coating is due to the uptake of electrolyte, which results in the set-up of conductive paths in the coatings.

Moreover, the blank coatings also possessed micropores that uptake water and ionic species from the electrolyte and initiate electrochemical corrosion reaction [55, 56]. The coating deterioration is also evident from the phase angle plot (Fig. 6d), in which the coatings can be seen as losing capacitance behavior. At the low-frequency range, the phase angle is nearly equal to 0° , and at the high-frequency range, the phase angle at 1st day of immersion demonstrates capacitance behavior. The impedance spectra possess two time constant as represented in an equivalent circuit (Fig. 6a) due to the accumulation of corrosion product between metal/coating interfaces [57]. The increase in the values of CPE1 and CPE2 is also an indication of the deterioration of the blank epoxy coating. The relationship between capacitance and resistance is inverse. The continuous decrease of barrier properties of coatings is attributed to the enhanced corrosion rate at the metal coating interface. The impedance value on the 20th day of immersion is decreased to $0.167 \text{ M}\Omega\cdot\text{cm}^2$ suggesting the decline in the protective barrier behavior of blank epoxy coatings.

The EIS spectra of capped HNTs/epoxy coatings (Fig. 6e, f) are different from those of blank epoxy coatings. The bode and phase angle plots of capped HNTs/epoxy coatings demonstrate better corrosion inhibition performance than the blank epoxy coatings. On the first day of immersion, the impedance value is $95.7 \text{ M}\Omega\cdot\text{cm}^2$, higher than that of blank epoxy

Figure 6 Equivalent circuit employed for fitting EIS data attained from EIS analysis of **a** Blank Epoxy coatings and **b** Capped HNTs/epoxy coatings. Bode and phase angle plots of **c, d** blank epoxy coatings and **e, f** capped HNTs/epoxy coatings after 20 days of immersion in 35 g/L NaCl solution.



coatings. However, a slight drop in the low-frequency impedance values is observed after five days of immersion but is still higher than that of blank epoxy coating. On the fifth day of immersion, the impedance value is monitored as $89.7 \text{ M}\Omega \cdot \text{cm}^2$ which may be due to the electrochemical reactions and corrosion activity due to the penetration of electrolyte through scratch [30, 58]. With the further increase in immersion time to ten days, the low-frequency impedance values are observed to increase. After the 20th day, the capped HNTs/epoxy coatings demonstrated good corrosion resistance behavior that is $1366 \text{ M}\Omega \cdot \text{cm}^2$. This considerable increase in corrosion resistance behavior is associated with the release of the inhibitor from HNTs due to the localized decrease in pH, which facilitates the breakdown of the metal-inhibitor bond and thus the release of the inhibitor.

With the increase in R_{ct} values, a considerable increase in W values is also seen due to the diffusion of functional species and the metal/coating interface.

Moreover, due to the addition of capped HNTs in the epoxy matrix, the mechanical properties of the matrix are also enhanced, as explained in Sect. "Electrochemical analysis of synthesized coatings". The phase angle plots of capped HNTs/epoxy (Fig. 6f) show that the coating exhibited capacitance behavior as the phase angle is near 85° , demonstrating the appropriate barrier properties of modified coatings. The corrosion inhibition efficiency of the capped HNTs/epoxy coatings as compared to the blank epoxy coatings can be computed utilizing the following equation [39],

$$IE(\%) = \frac{R_{ct}(\text{capped HNTs - epoxy coatings}) - R_{ct}(\text{blank epoxy coatings})}{R_{ct}(\text{capped HNTs - epoxy coatings})} \times 100 \quad (2)$$

The corrosion inhibition efficiency of capped HNTs/epoxy coatings after 20 days of immersion is 98% compared to the blank epoxy coatings.

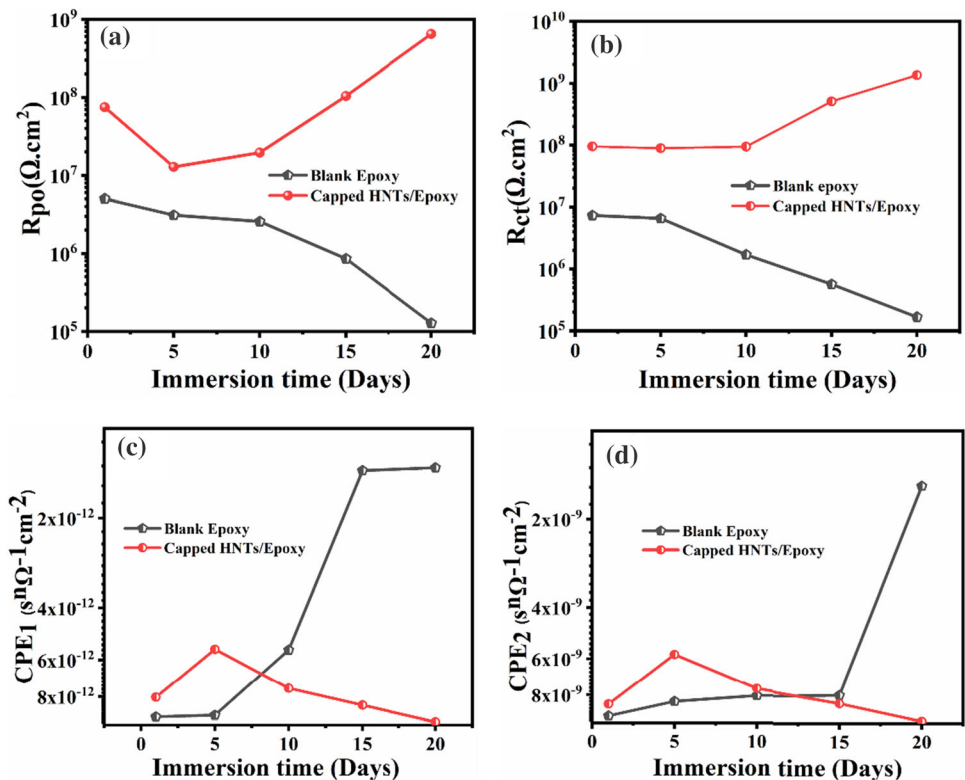
The evolution of the electrochemical parameters obtained after fitting EIS data of blank epoxy coatings and capped HNTs/epoxy coatings are represented in Fig. 7. The R_{pore} values of blank epoxy coatings are continuously decreasing, endorsing the deterioration of coating with the passage of immersion time. A similar decreasing trend in the R_{ct} values of blank epoxy coatings has been seen due to the uptake of electrolytes, as discussed above. This eventually leads to the delamination of coatings and thus no barrier between metal and electrolyte. The increase in the value of CPE1 and CPE2 of blank epoxy coatings over time indicates a complete decline in the corrosion barrier properties of coatings. But in the case of epoxy coatings modified by capped HNTs, the increasing trend in impedance values is seen after five days of immersion. This increase in R_p and R_{ct}

values with a decrease in CPE1 and CPE2 values indicates enhanced corrosion protection provided by modified coatings. This enhanced corrosion protection is related to the inhibitor's release from HNTs in the epoxy matrix. The detailed corrosion inhibition mechanism will be discussed in the next section. The photographs of the blank and modified capped HNTs epoxy coatings before and after immersion in NaCl solution for 20 days are provided in Figure S3. The blank epoxy coating deteriorated with time and finally degraded as seen in Fig. S3b, while the modified capped HNT epoxy coatings demonstrated better corrosion inhibition functionalities due to the inhibition effect of 8HQ as explained in mechanism section (Fig. S3D).

Corrosion inhibition mechanism of capped HNTs/epoxy coatings

The corrosion inhibition performance of the 8HQ (corrosion inhibitor) is primarily related to the nucleophilic reactive adsorption sites at oxygen and nitrogen, as represented in Fig. 8. 8HQ possesses two active adsorption spots involving oxygen and nitrogen [59]. When electrolyte interacts with the steel substrate corrosion process is initiated, electrons are

Figure 7 Evolution of EIS parameter obtained after fitting EIS data **a** R_{pore} **b** R_{ct} **c** CPE1 and **d** CPE2 during the immersion time of 20 days in 35 g/L NaCl solution.



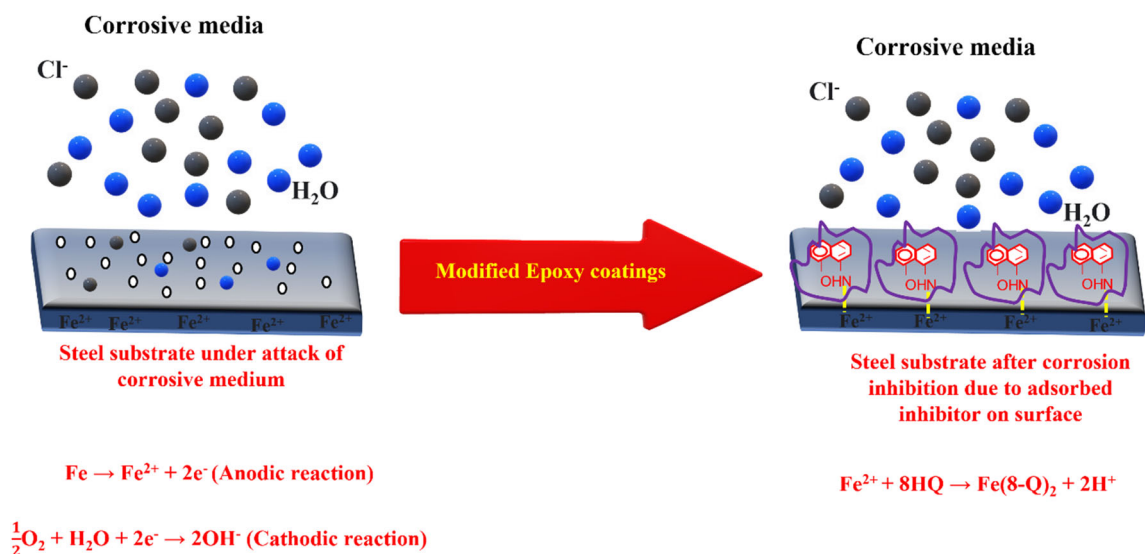
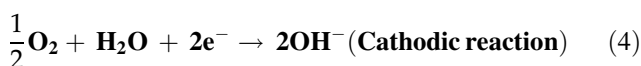
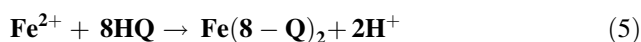


Figure 8 Schematics showing the corrosion inhibition mechanism provided by 8HQ on steel substrate after 20 days of immersion in 35 g/L NaCl solution.

transported from anode to cathode sites, releasing Fe^{2+} ions from steel substrate following the reactions [60].



Due to the initiation of corrosion at the anodic region, iron dissolution occurs, resulting in the localized change in pH at the scratch area. The pH at the scratch area is decreased due to the hydrolysis of Fe^{2+} . This decrease in pH provided H^+ ions which facilitated the breakdown of the metal-inhibitor bond at the ends of HNTs, as discussed in Sect. "UV-Vis spectroscopic analysis for release studies". This dissociation of Co (II) and inhibitor bond released 8HQ from the HNTs. The nucleophilic site of 8HQ then interacted with vacant d-orbitals of Fe (II) ions of steel substrate. It resulted in the formation of a coordinate covalent bond [61] of bis (8-hydroxyquinolinato) iron $\text{Fe}(\text{8-Q})_2$ as follows.



The adsorption of 8HQ from its reactive site on steel substrate formed a protective layer at the scratch area and thus prevented the further progression of the corrosion process. The onset of corrosion at an early stage is considered to be needed or important because it facilitates the initiation of acidification and further iron inhibitor ($\text{Fe}(\text{8-Q})_2$ complex formation,

which is formed by the interaction of nitrogen of 8HQ [62]. The XPS analysis also shows the adsorption of corrosion inhibitors on steel substrates, which will be discussed in the next section.

XPS analysis of the steel substrate after 120 h of immersion

The EIS results demonstrated the excellent barrier properties of modified epoxy coatings. The protective behavior of modified epoxy coatings is related to the adsorption of 8HQ on the metal surface due to the formation of the Fe-Inhibitor complex, as explained in Sect. 3.4.2. As stated, the XPS analysis technique was employed to validate the adsorption of 8HQ on metal. For this purpose, a modified (capped HNTs/Epoxy) coating was removed from the steel substrate after 120 h of immersion and was studied to examine the adsorption of the inhibitor. Figure 9 indicates the XPS spectra of the main elements observed on the steel substrate. The carbon (C1s) spectra are represented in Fig. 9a, deconvoluted into three distinctive peaks at 284.6, 285.2, and 287.6 eV. The binding energy peak at 284.6 eV is related to the C-C/C=C bond in the quinoline ring in 8HQ.

The peak at 285.2 eV is related to the C-H bond [63]. The peak at 286.6 eV relates to the C-O-C bonding, which corresponds to the bonding between epoxy molecules due to epoxy residue on steel substrate [56–58], or it can be of C-N bond aromatic ring

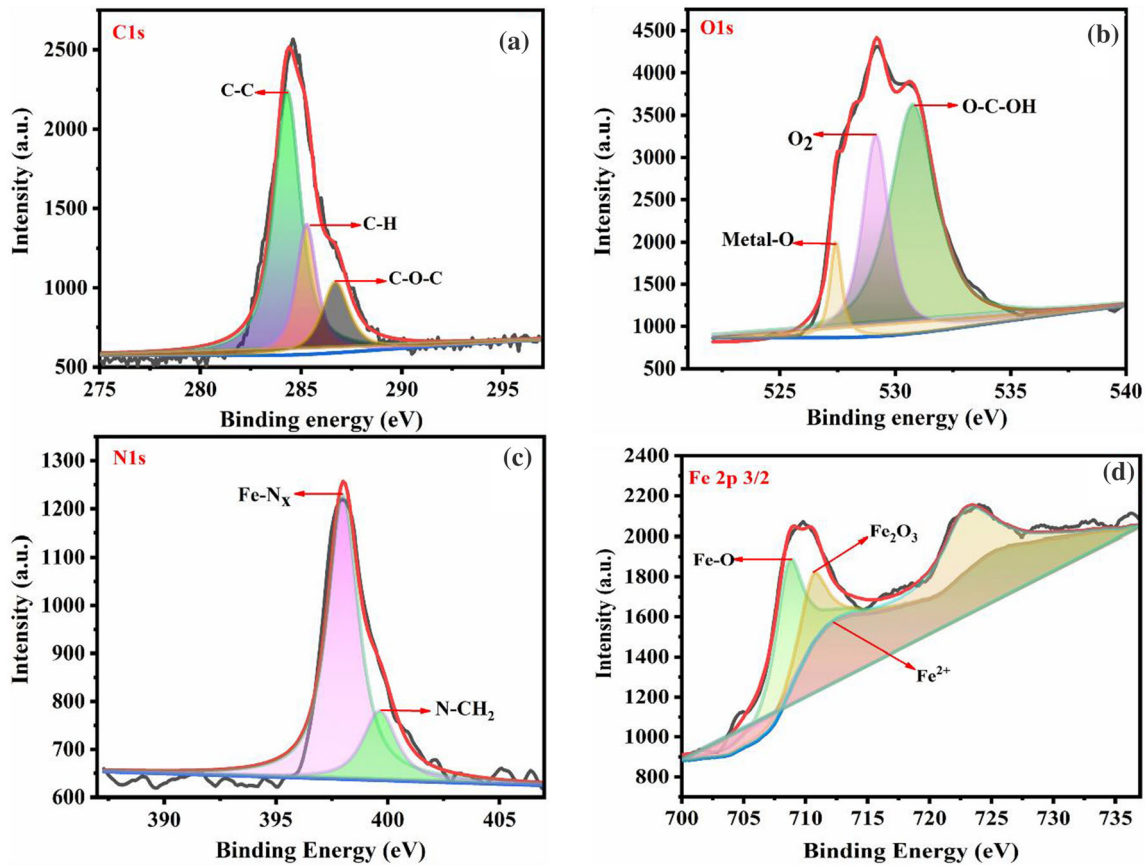


Figure 9 XPS analysis of steel surface after removal of coatings after 20 days of immersion. XPS spectra of **a** C1s, **b** O 1 s, **c** N 1 s and **d** Fe 2p 3/2.

Table 2 Elemental composition of the elements on the steel surface

Capped HNTs/epoxy coating steel surface	Surface composition of steel surface (Atomic %)			
	Carbon (C)	Oxygen (O)	Nitrogen (N)	Iron (Fe)
	53.46	31.12	8.09	7.31

of 8HQ [63]. The XPS spectra of oxygen (O 1 s) are represented in Fig. 9b. The oxygen spectra are fitted into three distinctive peaks at 529.1, 530.8, and 532.6 eV. The binding energy peak at 529.1 and 530.8 eV is related to the formation of a metal oxide bond, a Fe–O bond. The peak at 532.6 corresponds to the hydroxide formation, which may be iron hydroxide [63–65]. The N1s binding energy peaks are observed at 398.0 and 399.6 eV. The peak at 398.0 eV is related to the formation of Fe–N bonding, endorsing the adsorption mechanism claimed in Sect. 3.4.2. The peak at 399.6 is associated with N–C = in the quinoline ring and is consistent with previous studies [63, 64]. The XPS spectra of Fe 2p_{3/2} are deconvoluted into many peaks. Still, we represented three

distinctive peaks which can be observed at 709.0, 710.7, and 712.2 eV, related to the Fe (II) and Fe (III), which corresponds to the formation of metal oxide or hydroxide as observed in O1s spectra [66]. The elemental composition of elements observed through XPS analysis is also represented in Table 2. The existence of nitrogen in the composition confirmed the adsorption of 8HQ on the metal surface.

Conclusion

The work reported here demonstrated the synthesis of capped HNTs and their corrosion inhibition performance in the epoxy coating on steel substrate in

35 g/L NaCl solution. Quite a few conclusions obtained from this work are as follows.

1. Pristine HNTs were utilized to load 8HQ as corrosion inhibitor, followed by the capping of HNTs with Co (II) cap formation.
2. The capping of HNTs was established on the interaction of metal (Co) and inhibitor (8HQ) to form a metal-inhibitor complex.
3. The capped HNTs extended the release time of the inhibitor by 64% and made 8HQ available at the defect site by decomposing the metal-inhibitor complex.
4. TEM, FTIR, TGA, and UV–Vis spectroscopic analysis results endorsed the successful loading and modification of HNTs.
5. The tensile strength of modified epoxy coatings has been doubled due to the addition of capped HNTs compared to the blank epoxy coatings.
6. The epoxy coatings modified with capped HNTs also provided an excellent corrosion protection barrier with 98% corrosion inhibition efficiency compared to blank epoxy coatings due to the prolonged and efficient release of inhibitor from HNTs and formation Fe-inhibitor complex at the metal surface, thus providing extended corrosion protection in steel substrate at the defect site.
7. The utilization of Co (II) for capping of HNTs resulted in improved corrosion resistance performance of modified epoxy as compared to Cu (II) [31], which may be due to the more thermal stability of Co (II) as compared to that of Cu (II) [67] and more stable complex formation with Co (II).

In general, the capped HNTs/epoxy coatings reported in this work imply prospective and promising applications in the corrosion inhibition of steel substrate in a wide range of fields.

Acknowledgements

The authors would like to thank the Central laboratory Unit (CLU), Qatar University, 2713, Doha, Qatar, for the TEM analysis facility and the Gas processing center (GPC), Qatar University, 2713, Doha, for the XPS analysis faculty.

Author's contribution

Conceptualization, AK and SH; Methodology, SH; Software, SH, SM. I; Validation, SH; Formal Analysis, SH; Investigation, SH; Resources, AS, RK; Data Curation, SH; Writing—Original Draft Preparation, SH; Writing—Review & Editing, SH, AS; Visualization, SH.; Supervision, EMA, AS; Project Administration, AS, RK; Funding Acquisition, RK, AS.

Funding

Open access funding provided by the Qatar National Library. This research was funded by the Qatar National Research Fund (a member of the Qatar Foundation), grant number NPRP Grant 11S-1226-170132, NPRP Grant 13S-0120-200116 and Qatar University internal grant # QUCG-CENG-22/23-461. Statements made herein are solely the responsibility of the authors.

Data availability

The raw/processed data/code required to reproduce these findings cannot be shared at this time due to legal or ethical reasons.

Declarations

Conflict of interest The authors declare no conflict of interest.

Ethical approval Not applicable.

Supplementary Information: The online version contains supplementary material available at <http://doi.org/10.1007/s10853-023-08437-z>.

Open Access This article is licensed under a Creative Commons Attribution 4.0 International License, which permits use, sharing, adaptation, distribution and reproduction in any medium or format, as long as you give appropriate credit to the original author(s) and the source, provide a link to the Creative Commons licence, and indicate if changes were made. The images or other third party material in this article are included in the article's Creative Commons licence, unless indicated otherwise in a credit line to the material. If material is not included in the article's

Creative Commons licence and your intended use is not permitted by statutory regulation or exceeds the permitted use, you will need to obtain permission directly from the copyright holder. To view a copy of this licence, visit <http://creativecommons.org/licenses/by/4.0/>.

References

- [1] Finšgar M, Jackson J (2014) Application of corrosion inhibitors for steels in acidic media for the oil and gas industry: a review. *Corros Sci* 86:17–41. <https://doi.org/10.1016/j.corsci.2014.04.044>
- [2] He Y, Chen C, Xiao G, Zhong F, Wu Y, He Z (2019) Improved corrosion protection of waterborne epoxy/graphene coating by combining non-covalent and covalent bonds. *React Funct Polym* 137:104–115. <https://doi.org/10.1016/J.REACTFUNCTPOLYM.2019.02.001>
- [3] Qian B, Zheng Z, Michailids M, Fleck N, Bilton M, Song Y, Li G, Shchukin D (2019) Mussel-inspired self-healing coatings based on polydopamine-coated nanocontainers for corrosion protection. *ACS Appl Mater Interfaces* 11:10283–10291. https://doi.org/10.1021/ACSAMI.8B21197/SUPPL_FILE/AM8B21197_SI_001.PDF
- [4] Zahidah KA, Kakooei S, Ismail MC, Bothi Raja P (2017) Halloysite nanotubes as nanocontainer for smart coating application: a review. *Prog Org Coatings* 111:175–185. <https://doi.org/10.1016/J.PORGCOAT.2017.05.018>
- [5] Samadzadeh M, Boura SH, Peikari M, Kasiriha SM, Ashrafi A (2010) A review on self-healing coatings based on micro/nanocapsules. *Prog Org Coatings* 68:159–164. <https://doi.org/10.1016/J.PORGCOAT.2010.01.006>
- [6] Principles of corrosion engineering and corrosion control - Zaki Ahmad - Google books, (n.d.). https://books.google.com.qa/books?hl=en&lr=&id=10U1CRPV_BUC&oi=fnd&pg=PP2&ots=GDn6FinhtR&sig=y76xr3rQcIXu1-EHccLYAn7i1eA&redir_esc=y#v=onepage&q&f=false (Accessed Oct 9, 2018).
- [7] Wei H, Wang Y, Guo J, Shen NZ, Jiang D, Zhang X, Yan X, Zhu J, Wang Q, Shao L, Lin H, Wei S, Guo Z (2015) Advanced micro/nanocapsules for self-healing smart anticorrosion coatings. *J Mater Chem A* 3:469–480. <https://doi.org/10.1039/C4TA04791E>
- [8] Shchukin DG, Lamaka SV, Yasakau KA, Zheludkevich ML, Ferreira MGS, Möhwald H (2008) Active anticorrosion coatings with halloysite nanocontainers. *J Phys Chem C* 112:958–964. <https://doi.org/10.1021/jp076188r>
- [9] Chen C, He Y, Xiao G, Zhong F, Li H, Wu Y, Chen J (2019) Synergistic effect of graphene oxide@phosphate-intercalated hydroxalcite for improved anti-corrosion and self-healable protection of waterborne epoxy coating in salt environments. *J Mater Chem C* 7:2318–2326. <https://doi.org/10.1039/C8TC06487C>
- [10] Olivieri F, Castaldo R, Cocca M, Gentile G, Lavorgna M (2021) Innovative silver-based capping system for mesoporous silica nanocarriers able to exploit a twofold anticorrosive mechanism in composite polymer coatings: tailoring benzotriazole release and capturing chloride ions. *ACS Appl Mater Interfaces* 13:48141–48152. <https://doi.org/10.1021/acami.1c15231>
- [11] Olivieri F, Castaldo R, Cocca M, Gentile G, Lavorgna M (2021) Mesoporous silica nanoparticles as carriers of active agents for smart anticorrosive organic coatings: a critical review. *Nanoscale* 13:9091–9111. <https://doi.org/10.1039/D1NR01899J>
- [12] Castaldo R, de Luna MS, Siviello C, Gentile G, Lavorgna M, Amendola E, Cocca M (2020) On the acid-responsive release of benzotriazole from engineered mesoporous silica nanoparticles for corrosion protection of metal surfaces. *J Cult Herit* 44:317–324. <https://doi.org/10.1016/j.culher.2020.01.016>
- [13] Cui M, Ren S, Chen J, Liu S, Zhang G, Zhao H, Wang L, Xue Q (2017) Anticorrosive performance of waterborne epoxy coatings containing water-dispersible hexagonal boron nitride (h-BN) nanosheets. *Appl Surf Sci* 397:77–86. <https://doi.org/10.1016/J.APSUSC.2016.11.141>
- [14] Abdullayev E, Abbasov V, Tursunbayeva A, Portnov V, Ibrahimov H, Mukhtarova G, Lvov Y (2013) Self-healing coatings based on halloysite clay polymer composites for protection of copper alloys. *ACS Appl Mater Interfaces* 5:4464–4471. https://doi.org/10.1021/AM400936M/SUPPL_FILE/AM400936M_SI_001.PDF
- [15] Hao Y, Zhao Y, Yang X, Hu B, Ye S, Song L, Li R (2019) Self-healing epoxy coating loaded with phytic acid doped polyaniline nanofibers impregnated with benzotriazole for Q235 carbon steel. *Corros Sci* 151:175–189. <https://doi.org/10.1016/J.CORSCI.2019.02.023>
- [16] Liu M, Jia Z, Jia D, Zhou C (2014) Recent advance in research on halloysite nanotubes-polymer nanocomposite. *Prog Polym Sci* 39:1498–1525. <https://doi.org/10.1016/J.PROGPOLYMSCI.2014.04.004>
- [17] Asadi N, Naderi R, Mahdavian M (2019) Halloysite nanotubes loaded with imidazole dicarboxylic acid to enhance protection properties of a polymer coating. *Prog Org Coatings* 127:375–384. <https://doi.org/10.1016/j.porgcoat.2018.11.035>
- [18] Lazzara G, Cavallaro G, Panchal A, Fakhrullin R, Stavitskaya A, Vinokurov V, Lvov Y (2018) An assembly of organic-inorganic composites using halloysite clay

- nanotubes. *Curr Opin Colloid Interface Sci* 35:42–50. <https://doi.org/10.1016/J.COCIS.2018.01.002>
- [19] Yuan P, Tan D, Annabi-Bergaya F (2015) Properties and applications of halloysite nanotubes: recent research advances and future prospects. *Appl Clay Sci* 112–113:75–93. <https://doi.org/10.1016/J.CLAY.2015.05.001>
- [20] Cipurković A, Horozić E, Marić S, Mekić L, Junuzović H (2021) Metal complexes with 8-Hydroxyquinoline: synthesis and *In Vitro* antimicrobial activity, open. *J Appl Sci* 11:1–10. <https://doi.org/10.4236/ojapps.2021.111001>
- [21] Sgarlata C, Arena G, Bonomo RP, Giuffrida A, Tabbi G (2018) Simple and mixed complexes of copper(II) with 8-hydroxyquinoline derivatives and amino acids: characterization in solution and potential biological implications. *J Inorg Biochem* 180:89–100. <https://doi.org/10.1016/j.jinorgbio.2017.12.002>
- [22] Duarte HA, Lourenço MP, Heine T, Guimarães L (2012) Clay mineral nanotubes: stability, structure and properties, stoichiometry. *Mater Sci - When Numbers Matter*. <https://doi.org/10.5772/34459>
- [23] Borisova D, Möhwald H, Shchukin DG (2013) Influence of embedded nanocontainers on the efficiency of active anti-corrosive coatings for aluminum alloys part II: influence of nanocontainer position. *ACS Appl Mater Interfaces* 5:80–87. https://doi.org/10.1021/AM302141Y/SUPPL_FILE/AM302141Y_SI_001.PDF
- [24] Li GL, Zheng Z, Möhwald H, Shchukin DG (2013) Silica/polymer double-walled hybrid nanotubes: synthesis and application as stimuli-responsive nanocontainers in self-healing coatings. *ACS Nano* 7:2470–2478. <https://doi.org/10.1021/nn305814q>
- [25] Tully J, Yendluri R, Lvov Y (2016) Halloysite clay nanotubes for enzyme immobilization. *Biomacromol* 17:615–621. <https://doi.org/10.1021/acs.biomac.5b01542>
- [26] Cavallaro G, Lazzara G, Massaro M, Milioto S, Noto R, Parisi F, Riela S (2015) Biocompatible Poly(N-isopropylacrylamide)-halloysite nanotubes for thermoresponsive curcumin release. *J Phys Chem C* 119:8944–8951. <https://doi.org/10.1021/ACS.JPCC.5B00991>
- [27] Joshi A, Abdullayev E, Vasiliev A, Volkova O, Lvov Y (2013) Interfacial modification of clay nanotubes for the sustained release of corrosion inhibitors. *Langmuir* 29:7439–7448. <https://doi.org/10.1021/la3044973>
- [28] Dзамukова MR, Naumenko EA, Lvov YM, Fakhruullin RF (2015) Enzyme-activated intracellular drug delivery with tubule clay nanoformulation. *Sci Reports* 5(5):1–11. <https://doi.org/10.1038/srep10560>
- [29] Lvov Y, Wang W, Zhang L, Fakhruullin R (2016) Halloysite clay nanotubes for loading and sustained release of functional compounds. *Adv Mater* 28:1227–1250. <https://doi.org/10.1002/ADMA.201502341>
- [30] Xing X, Zhou D, Tang E, Liu S, Chu X, Xu X, Xu Y (2020) A novel method to control the release rate of halloysite encapsulated Na₂MoO₄ with Ca²⁺ and corrosion resistance for Q235 steel. *Appl Clay Sci* 188:105492. <https://doi.org/10.1016/j.clay.2020.105492>
- [31] Wang M, Wang J, Hu W (2020) Preparation and corrosion behavior of Cu-8-HQ@HNTs/epoxy coating. *Prog Org Coatings* 139:105434. <https://doi.org/10.1016/j.porgcoat.2019.105434>
- [32] Gao H, Li Q, Dai Y, Luo F, Zhang HX (2010) High efficiency corrosion inhibitor 8-hydroxyquinoline and its synergistic effect with sodium dodecylbenzenesulphonate on AZ91D magnesium alloy. *Corros Sci* 52:1603–1609
- [33] S V Lamaka, ML Zheludkevich, KA Yasakau, MF Montemor, MGS (2007) Ferreira, High effective organic corrosion inhibitors for 2024 aluminium alloy. 52: 7231–7247. <https://doi.org/10.1016/j.electacta.2007.05.058>
- [34] Obot IB, Anka NK, Sorour AA, Gasem ZM, Haruna K (2017) 8-Hydroxyquinoline as an alternative green and sustainable acidizing oilfield corrosion inhibitor, sustain. *Mater Technol* 14:1–10
- [35] Verma C, Olasunkanmi LO, Obot IB, Ebenso EE, Quraishi MA (2016) 5-Arylpyrimido-[4, 5-b] quinoxaline-diones as new and sustainable corrosion inhibitors for mild steel in 1 M HCl: a combined experimental and theoretical approach. *RSC Adv* 6:15639–15654
- [36] S Muthaiah, A Bhatia, M Kannan (2020) Stability of metal complexes. In: A N Srivastava (Ed.), *IntechOpen*, Rijeka, 2020: p Ch 2. <https://doi.org/10.5772/intechopen.90894>
- [37] Abdullayev E, Lvov Y (2011) Halloysite clay nanotubes for controlled release of protective agents. *J Nanosci Nanotechnol* 11:10007–10026. <https://doi.org/10.1166/jnn.2011.5724>
- [38] Hebbar RS, Isloor AM, Zulhairun AK, Sohaimi Abdullah M, Ismail AF (2017) Efficient treatment of hazardous reactive dye effluents through antifouling polyetherimide hollow fiber membrane embedded with functionalized halloysite nanotubes. *J Taiwan Inst Chem Eng* 72:244–252. <https://doi.org/10.1016/j.jtice.2017.01.022>
- [39] Khan A, Hassanein A, Habib S, Nawaz M, Shakoor RA, Kahraman R (2020) Hybrid halloysite nanotubes as smart carriers for corrosion protection. *ACS Appl Mater Interfaces* 12:37571–37584. <https://doi.org/10.1021/acsami.0c08953>
- [40] Chiter F, Lacaze-Dufaure C, Tang H, Pébère N (2015) DFT studies of the bonding mechanism of 8-hydroxyquinoline and derivatives on the (111) aluminum surface. *Phys Chem Chem Phys* 17:22243–22258. <https://doi.org/10.1039/c5cp03095a>

- [41] Chen C, Xiao G, He Y, Zhong F, Li H, Wu Y, Chen J (2020) Bio-inspired superior barrier self-healing coating: Self-assemble of graphene oxide and polydopamine-coated halloysite nanotubes for enhancing corrosion resistance of waterborne epoxy coating. *Prog Org Coatings* 1(139):105402. <https://doi.org/10.1016/j.porgcoat.2019.105402>
- [42] Asadi N, Naderi R, Mahdavian M (2019) Doping of zinc cations in chemically modified halloysite nanotubes to improve protection function of an epoxy ester coating. *Corros Sci* 151:69–80. <https://doi.org/10.1016/j.corsci.2019.02.022>
- [43] Aravinth K, Anandha Babu G, Ramasamy P (2012) Growth of 2018 hydroxyquinoline organic crystal by Czochralski method and its characterizations. *J Therm Anal Calorim* 110:1333–1339. <https://doi.org/10.1007/s10973-011-2121-5>
- [44] Xing X, Wang J, Li Q, Hu W, Yuan J (2018) A novel acid-responsive HNTs-based corrosion inhibitor for protection of carbon steel. *Colloids Surf A Physicochem Eng Asp* 553:295–304. <https://doi.org/10.1016/j.colsurfa.2018.05.072>
- [45] Fung MK, Ng AMC, Djurišić AB, Chan WK, Wang H (2012) Preparation of 8-hydroxyquinoline wires by decomposition of tris(8-hydroxyquinoline) aluminium. *J Exp Nanosci* 7:578–585. <https://doi.org/10.1080/17458080.2010.543992>
- [46] Li H, Li Y (2009) Synthesis of highly luminescent cobalt(ii)-bis(8-hydroxyquinoline) nanosheets as isomeric aromatic amine probes. *Nanoscale* 1:128–132. <https://doi.org/10.1039/b9nr00019d>
- [47] Yuan P, Tan D, Annabi-Bergaya F, Yan W, Fan M, Liu D, He H (2012) Changes in structure, morphology, porosity, and surface activity of mesoporous halloysite nanotubes under heating. *Clays Clay Miner* 60:561–573. <https://doi.org/10.1346/CCMN.2012.0600602>
- [48] A Zhang, Y Zhang, Z Zhu (2019) Thermal properties of Halloysite nanotubes (HNTs) intercalation complexes—a review. *E3S Web Conf* <https://doi.org/10.1051/e3sconf/201913101055>.
- [49] Patel KD, Patel HS (2017) Synthesis, spectroscopic characterization and thermal studies of some divalent transition metal complexes of 8-hydroxyquinoline. *Arab J Chem* 10:S1328–S1335. <https://doi.org/10.1016/j.arabjc.2013.03.019>
- [50] Degeiso RC, Donaruma LG, Tomic EA (1965) Preparation and chelating properties of 8-hydroxy-quinoline—formaldehyde polymers. *J Appl Polym Sci* 9:411–419. <https://doi.org/10.1002/app.1965.070090202>
- [51] Habib S, Fayyad E, Nawaz M, Khan A, Shakoor RA, Kahraman R, Abdullah A (2020) Cerium dioxide nanoparticles as smart carriers for self-healing coatings. *Nanomaterials* 10(4):791. <https://doi.org/10.3390/nano10040791>
- [52] Freitas AR, Silva M, Ramos ML, Justino LLG, Fonseca SM, Barsan MM, Brett CMA, Silva MR, Burrows HD (2015) Synthesis, structure, and spectral and electrochemical properties of chromium(iii) tris-(8-hydroxyquinolate). *Dalt Trans* 44:11491–11503. <https://doi.org/10.1039/C5DT00727E>
- [53] Zhu C, Wang Y, Mao Q, Li F, Li Y, Chen C (2017) Two 8-hydroxyquinolate based supramolecular coordination compounds: Synthesis, structures and spectral properties. *Materials* 10(3):313. <https://doi.org/10.3390/ma10030313>
- [54] Xing X, Xu X, Wang J, Hu W (2019) Preparation, release and anticorrosion behavior of a multi-corrosion inhibitors-halloysite nanocomposite. *Chem Phys Lett* 718:69–73. <https://doi.org/10.1016/j.cplett.2019.01.033>
- [55] Mafi R, Mirabedini SM, Naderi R, Attar MM (2008) Effect of curing characterization on the corrosion performance of polyester and polyester/epoxy powder coatings. *Corros Sci* 50:3280–3286. <https://doi.org/10.1016/j.corsci.2008.08.037>
- [56] Schem M, Schmidt T, Gerwonn J, Wittmar M, Veith M, Thompson GE, Molchan IS, Hashimoto T, Skeldon P, Phani AR, Santucci S, Zheludkevich ML (2009) CeO₂-filled sol-gel coatings for corrosion protection of AA2024-T3 aluminium alloy. *Corros Sci* 51:2304–2315. <https://doi.org/10.1016/j.corsci.2009.06.007>
- [57] Habib S, Fayyad E, Nawaz M, Khan A, Shakoor RA, Kahraman R, Abdullah A (2020) Cerium dioxide nanoparticles as smart carriers for self-healing coatings. *Nanomaterials*. <https://doi.org/10.3390/nano10040791>
- [58] Habib S, Fayyad E, Shakoor RA, Kahraman R, Abdullah A (2021) Improved self-healing performance of polymeric nanocomposites reinforced with talc nanoparticles (TNPs) and urea-formaldehyde microcapsules (UFMCs). *Arab J Chem* 14(2):102926. <https://doi.org/10.1016/j.arabjc.2020.102926>
- [59] Al Zoubi W, Ko YG (2019) Self-assembly of hierarchical N-heterocycles-inorganic materials into three-dimensional structure for superior corrosion protection. *Chem Eng J* 15(356):850–856. <https://doi.org/10.1016/j.cej.2018.09.089>
- [60] Söylev TA, Richardson MG (2008) Corrosion inhibitors for steel in concrete: state-of-the-art report. *Constr Build Mater* 22:609–622. <https://doi.org/10.1016/j.conbuildmat.2006.10.013>
- [61] Ryu H-S, Singh JK, Yang H-M, Lee H-S, Ismail MA (2016) Evaluation of corrosion resistance properties of N, N'-Dimethyl ethanolamine corrosion inhibitor in saturated Ca (OH) 2 solution with different concentrations of chloride

- ions by electrochemical experiments. *Constr Build Mater* 114:223–231
- [62] Attaei M, Taryba MG, Shakoor RA, Kahraman R, Marques AC, Montemor MF (2022) Highly protective polyolefin coating modified with ceria nano particles treated with N, N, N', N'-Tetrakis (2-hydroxyethyl) ethylenediamine for corrosion protection of carbon steel. *Corrosion Sci* 15(198):110162. <https://doi.org/10.1016/j.corsci.2022.110162>
- [63] Wang X, Li L, Xie Z-H, Yu G (2018) Duplex coating combining layered double hydroxide and 8-quinolinol layers on Mg alloy for corrosion protection. *Electrochim Acta* 283:1845–1857. <https://doi.org/10.1016/j.electacta.2018.07.113>
- [64] Nawaz M, Naeem N, Kahraman R, Montemor MF, Haider W, Shakoor RA (2021) Effectiveness of epoxy coating modified with yttrium oxide loaded with imidazole on the corrosion protection of steel. *Nanomaterials* 11:1–16. <https://doi.org/10.3390/nano11092291>
- [65] Wang DH, Hu Y, Zhao JJ, Zeng LL, Tao XM, Chen W (2014) Holey reduced graphene oxide nanosheets for high performance room temperature gas sensing. *J Mater Chem A* 2:17415–17420
- [66] Miller DJ, Biesinger MC, McIntyre NS (2002) Interactions of CO₂ and CO at fractional atmosphere pressures with iron and iron oxide surfaces: One possible mechanism for surface contamination? *Surf Interface Anal* 33:299–305. <https://doi.org/10.1002/sia.1188>
- [67] Świdorski G, Łażny R, Sienkiewicz M, Kalinowska M, Świsłocka R, Acar AO, Golonko A, Matejczyk M, Lewandowski W (2021) Synthesis, spectroscopic, and theoretical study of copper and cobalt complexes with dacarbazine. *Materials (Basel)* 14:1–21. <https://doi.org/10.3390/ma14123274>

Publisher's Note Springer Nature remains neutral with regard to jurisdictional claims in published maps and institutional affiliations.